Advanced Powder Technology 26 (2015) 470–477

Contents lists available at ScienceDirect

Advanced Powder Technology

journal homepage: www.elsevier.com/locate/apt

Original Research Paper

A detailed study of phase evolution in Cu–16 at. %Al and Cu–30 at. %Al alloys under different types of mechanical alloying processes

M.F. Giordana [a,*], M.R. Esquivel [a,b], E. Zelaya [a]

[a] CONICET, Centro Atómico Bariloche, CNEA, Av. Bustillo 9500, 8400 S.C. de Bariloche, Argentina
[b] Centro Regional Universitario Bariloche, Universidad Nacional del Comahue, Quintral 1250, 8400 S.C. de Bariloche, Argentina

ARTICLE INFO

Article history:
Received 11 September 2014
Received in revised form 2 December 2014
Accepted 5 December 2014
Available online 18 December 2014

Keywords:
Intermetallics
Mechanical alloying and milling
Powder metallurgy
X-ray diffraction
Transmission electron microscopy

ABSTRACT

The phase stability of Cu–16 at. %Al and Cu–30 at. %Al alloys obtained by a planetary and an horizontal mills was investigated. The analysis was carried out using X-ray diffraction and various transmission electron microscopy (TEM) techniques. X-ray diffraction analysis gives a statistical overview of the main equilibrium phases present. Meanwhile, the different TEM techniques allow the detection of either the minor phases or the ones having crystalline domains smaller than 5 nm. The solid solution equilibrium α phase was obtained using both milling processes on the Cu–16 at. %Al. Instead, the final intermetallics observed for Cu–30 at. %Al were not the equilibrium ones according to the phase diagram. The planetary mill produced a mixture of α and γ_2 phases and less than a 2 at. % of β phase. The horizontal mill produced a γ_2 phase and less than a 2 at. % of α_2 and γ phases. For both compositions, the horizontal mill seems to be more efficient to achieved the equilibrium intermetallic compound.

1. Introduction

There are many techniques for the synthesis and the production of materials on non-equilibrium conditions [1]. Among them, it is worth to mention plasma processing [1,2], rapid solidification processing [3,4] and vapor deposition [1,5]. Despite the advantages reported on these, mechanical alloying method (MA) [1,6] is one of the most widely used. Low cost and simplicity of production are among the main advantages of this method. MA is specially useful to synthesize alloys with components with large difference in melting temperature. The process should avoid the mass loss of the component with the lower melting temperature because synthesis is done near room temperature. MA is a powder processing technique characterized by a cycle of repeated welding and fracturing of the powder particles inside a mill. The following changes can be produced by MA (i) structural changes, such as alterations in composition and lattice parameters, (ii) microstructural changes, such as a variation in particle size or grain size and amorphization, (iii) change of solubility boundaries in the phase diagram [6]. Depending on the milling conditions, the intermetallics formation is produced near room temperature. Therefore, the phase equilibrium showed in a phase diagram might not be reconstructed by MA processes [7]. As an example, systems with the same level of metastability of phases like Cu–Zn and Ni–Al did not produced stable phases according to the phase diagrams for the analyzed compositions [8–10].

The processing of Al–Cu by MA was widely studied over the last decade. Nevertheless, most of the effort was focused on a composition near to Cu–98 at. %Al, varying the type of dispersoid [11–14]. This composition is of great interest because the alloy has a specific mass close to the Al one but with higher hardness and toughness. The addition of dispersoids also aims to improve the hardness of the obtained intermetallic. Otherwise, only few reported works are based on compositions between Cu–16 at. %Al and Cu–30 at. %Al. Samal et al. [15] studied the microstructure of Cu–25 at. %Al alloy produced by a planetary ball mill. They obtained ultrafined Cu–Al particles after 50 h of milling. They found that the Al–Cu solid state reaction; i.e. the alloy formation, starts after 10 h milling. However, no additional information was reported about the structure of the produced intermetallics. The lack of references for compositions between Cu–16 at. %Al and Cu–30 at. %Al may be due to the complexity exhibited by the Cu–Al phase diagram in this region.

Fig. 1 shows the Cu–Al equilibrium phase diagram between 15 and 35 atomic percent of aluminum. It is expected to found the cubic α phase for Cu–16 at. %Al [7,16]. The α phase is disordered and presents the same space group than Cu. The phase has a slightly larger lattice parameter due to the Cu substitutional replacement by a larger Al atom [17]. For higher Al concentrations,

* Corresponding author. Tel.: +54 2944 445548; fax: +54 2944 445299.
E-mail address: florencia.giordana@cab.cnea.gov.ar (M.F. Giordana).

http://dx.doi.org/10.1016/j.apt.2014.12.005
0921-8831/

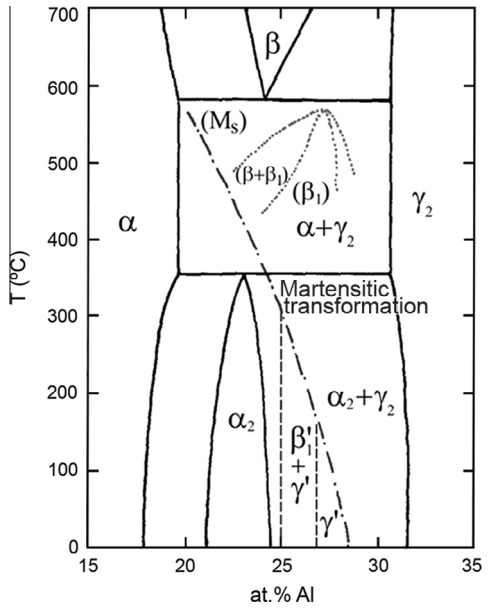

Fig. 1. Phase diagram for Cu–Al alloys (continuous lines), M_s temperatures and regions of the stability of the different martensitic phases [2].

around Cu–23 at. %Al and below 350 °C, the compact and tetragonal α_2 is the stable phase [17,18]. Reaching Cu–30 at. %Al, the phase diagram indicates the coexistence of the α_2 structure with the cubic γ_2 phase. γ_2 could be either an ordered or a disordered structure [19]. The unit cell contains a total of 52 atoms and 2 structural vacancies with a lattice parameter larger than three times the one of α.

The metastable phase β (CsCl-type, ordered bcc) could be retained by quenching alloys with compositions between Cu–22 at. %Al and Cu–27 at. %Al [17,20]. This phase undergoes a martensitic reversible transformation induced by temperature or stress. It changes to either γ′ or β_1' phases depending on the composition [21,22]. As observed in Fig. 1, there is a sharp variation of the temperature of martensitic transformation with the alloy composition. γ′ and β_1', also defined as low temperature phases, are both closed packed ones with multiple stacking faults. γ′ could be described as an hexagonal phase or 2H with an AB staking sequence [17], while the β_1' could be described as a monoclinic phase (9R or 18R) with a ABCBCACAB staking sequence [18,23].

Cold compact and hot rolling pre alloyed powders is one of the common processing routes used to obtain shape memory alloys. These alloys have a high percentage of two-way shape memory strain and high average fracture stress [24,25]. The milled powders used in these processes should achieve the formation of intermetallics [24]. Therefore, it is important to analyze in detail the evolution of phase formation under different milling conditions. The main purpose of the present work is to characterize the phase evolution of the powders for the Cu–16 at. %Al and Cu–30 at. %Al alloys obtained by medium and low energy ball mills.

The powders were analyzed using X-ray diffraction (XRD) and transmission electron microscopy (TEM). The first technique allows a statistical analysis of the presence of the main phases. The second one is also able to detect minor phases existing in smaller crystallographic domains due to a threshold better than 1 nm [26,27].

2. Material and methods

The mixture of elemental Cu (99.999% purity) and Al (99.5% purity) powders in ratios of Cu–16 at. %Al and Cu–30 at. %Al were mechanically alloyed using two different ball mills. Measurements were done in Ar atmosphere (99.999%) at controlled conditions (humidity < 100 ppm, O_2 content < 5 ppm). The elemental blends were mechanically alloyed in a planetary-motioned mill Fritsch pulverissette 6 (PM). This device is considered a medium-energy milling [6,28,29]. Blends were also milled in an horizontally-motioned mill Uniball Mill II-Australian Instruments (HM). This device is considered a low-energy milling device [6,10,30]. Magnet positions were bellow the chamber and bellow the right lower side of the chamber. These position maximize the amount of impact energy since the balls are made of magnetic steel. Both milling processes were carried out in stainless steel chamber with stainless steel balls. Milling speeds selected were 120 rpm for PM and 140 rpm for HM. A ball/sample mass ratio of 8.25:1 and 22.33:1 were chosen for PM and for HM, respectively. After certain intervals of time, samples were withdrawn from the chamber for XRD and TEM analysis. Sampling was done by keeping approximately the same ball/mass ratio. For PM, the integrated milling times (t_{im}) were 10, 20, 30 and 50 h. For HM, t_{im} selected were 10, 30, 50 and 100 h. Additionally, intermediate times of 12 and 15 h were employed for the nominal composition Cu–30 at. %Al. Tables 1 and 2 present the nomenclature used for the different samples.

Table 1
Nomenclature for Cu–16 at. %Al samples depending on the motioned-type of mill and integrated milling time and general characteristics of XRD and TEM.

Sample	t_{im} (h)	Mill type	XRD	TEM
16-PM-10	10	Planetary	Cu + Al	Cu + Al
16-PM-20	20	Planetary	Cu + Al	α
16-PM-30	30	Planetary	α	α
16-PM-50	50	Planetary	α	α
16-HM-10	10	Horizontal	Cu + Al	Cu + Al
16-HM-30	30	Horizontal	α	α
16-HM-50	50	Horizontal	α	α
16-HM-100	100	Horizontal	α	α

Table 2
Nomenclature for Cu–30 at. %Al samples depending on the motioned-type of mill and integrated milling time and general characteristics of XRD and TEM analysis.

Sample	t_{im} (h)	Mill type	XRD	TEM
30-PM-10	10	Planetary	Cu + Al	Cu + Al
30-PM-20	20	Planetary	α + γ_2	α + γ_2
30-PM-30	30	Planetary	α + γ_2	α + γ_2
30-PM-50	50	Planetary	α + γ_2	α + γ_2 + β
30-HM-10	10	Horizontal	Cu + Al	Cu + Al
30-HM-12	12	Horizontal	α + γ_2	α + γ2 + Al
30-HM-15	15	Horizontal	α + γ_2	α + γ2 + Al
30-HM-30	30	Horizontal	α + γ_2	α + γ2 + Al
30-HM-50	50	Horizontal	γ_2	γ_2
30-HM-100	100	Horizontal	γ_2	γ_2 + α_2 + γ′

Powders were characterized by room temperature X-ray diffraction using a Philips PW 1710/01 and a PANalytical X'Pert Instruments with Cu Kα radiation. Characterization of the X-ray profiles and mass ratio estimation were done by the Rietveld method using Fullprof program [31,32]. TEM characterization was performed using a TEM FEI CM200 UT and a TEM FEI Tecnai F20 G2 with field emission gun, both operated at 200 kV.

3. Results

3.1. Phase evolution of Cu–16 at. %Al

3.1.1. X-ray diffraction patterns

At the shortest milling time, X-ray diffractograms corresponding to samples 16-PM-10 and 16-HM-10 could be indexed consid-

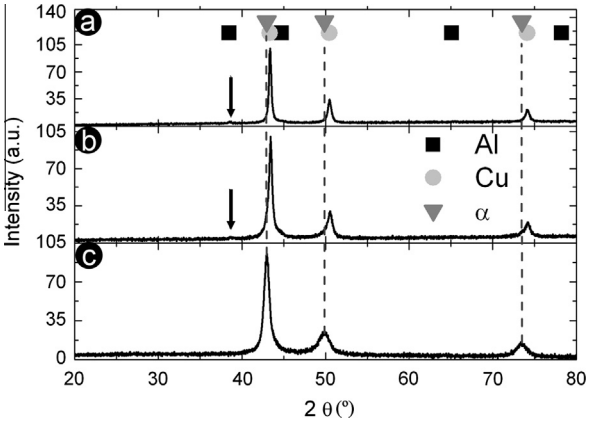

Fig. 2. X-ray diffractograms of Cu–16 at. %Al milled in planetary ball mill for (a) 10 h (b) 20 h and 50 h.

ering the presence of Cu and Al disaggregated. The same result was obtained for the powder milled for 20 h in PM. To the detection limit of the technique, no peaks are attributed to an intermetallic phase. At longer milling times, all the peaks on the XRD patterns for this composition could be indexed considering only the cubic α phase as presented in Table 1 and Fig. 2. XRD results for longer integrated milling times are in agreement with the phase predicted by the phase diagram shown in Fig. 1. In this figure, α phase appears at room temperature for 16 at. %Al. As observed in Fig. 2, the FWHM of the peaks increases as milling progresses. Neither XRD peak identification nor TEM EDS reveals any contamination of vial elements or previous milling in the particles analyzed.

3.1.2. TEM observations

The detailed study of the powders was performed using TEM by analizing a significative amount of particles. The most representative way to study the existence of phases in the TEM is selected area diffraction (SAD) analysis. This technique has a better detection limit than XRD and allows to find minor phases among the main ones detected by XRD [26,27]. An outline of the phases identified according to each technique is presented in Table 1.

One of the advantages of the TEM is the possibility to perform highly localized studies. For example. It allows to observe differences inside particles of a few hundred nanometers in diameter. Fig. 3(a) shows a particle of 16-PM-10 sample. In this particle, it was performed a differential compositional study through Energy Dispersive Spectrometry (EDS) in two different areas with a spot-size lower than 10 nm. A zoom of the region where both EDS were performed are shown in Fig. 3(b). The EDS was performed in both zones pointed with arrows in Fig. 3(b). Those are exhibited in Fig. 3(c). A quantification using MThin method of EDAX Genesis spectrum software was performed for each area. A depletion of 17 at. %Al was detected in the first area respect to the second one. This kind of inhomogeneity was not observed in particles milled for longer times using the same spot size.

For 10 h milling in PM, it was possible to index the SAD patterns taking into account the presence of Cu and Al. The same results were obtained for XRD pattern. After 20 h, a difference between XRD and SAD was detected. For the sample 16-PM-20, X-ray diffractogram seemed to show the presence of Cu and Al. Instead, it was only possible to associate the α phase to the SAD patterns by TEM. For 30 and 50 h of milling, it was observed an agreement between XRD and SAD phase identification. In both cases, it was possible to explain the identities assigned to all rings by only considering the existence of α phase.

For HM, TEM and XRD seems to be in complete agreement. For the sample 16-HM-10, the selected area diffraction patterns could

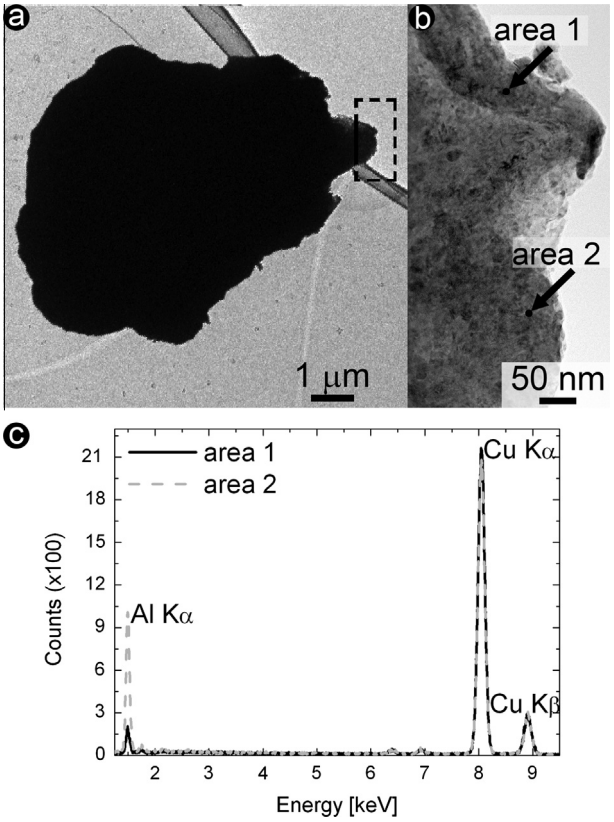

Fig. 3. (a) TEM bright field image of the sample 16-PM-10. (b) Magnified micrograph of the rectangle area shown in (a). (c) EDS spectrum of areas pointed with arrows in (b).

be indexed as Cu and Al. For the others samples, i.e. 16-HM-30, 16-HM-50, 16-HM-100, SAD patterns appeared to be consistent only with the presence of α phase.

3.2. Phase evolution of Cu–30 at. %Al

3.2.1. X-ray diffraction patterns

During MA, the elemental blends seem to evolved into two different intermetallics, α and γ_2. The final mass ratio of those intermetallics was not the same for each type of mill. On the one hand, Fig. 4(a) shows the evolution of X-ray diffractograms corresponding to planetary ball mill for the different integrated milling times. For the sample 30-PM-10, XRD pattern shows the presence of Cu and Al. Milling for longer t_{im} resulted in samples consistent with the presence of a mixture of α and γ_2 phases. After 50 h milling, the highest peak at 43.00° is related to the α phase, and not to the γ_2 phase.

On the other hand, the results obtained for the horizontal ball milling are showed in Fig. 4(b). The 30-HM-10 diffractogram was similar to the one of 30-PM-10. It was indexed considering only Cu and Al. For the second t_{im} studied, 12 h, the diffractogram was indexed considering α and γ_2 phases. The highest peak of 30-HM-10 is at 2θ value of 43.36°. It seemed to stand for the most significant peak of each phase, 43.00° and 44.11°. For 30-HM-12, the highest one was related to α phase. As milling evolved, the relative height of the main peaks of each phase started to invert the tendency. The highest main peak was of γ_2 phase for 30-HM-30. This trend continued during the milling by reaching the disappearance of the peaks associated to α phase after 50 h milling. Finally, XRD results for 30-HM-100 shown only γ_2 phase. Also here, nor XRD peak or TEM EDS reveals any contamination of vial elements or previous milling in the particles studied.

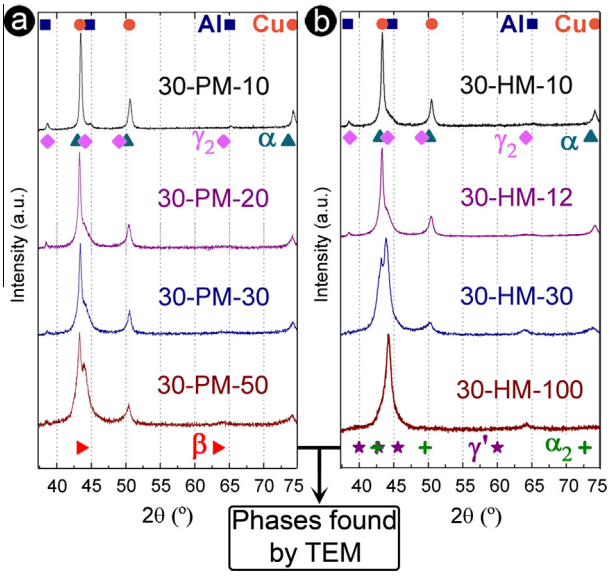

Fig. 4. X-ray diffractograms of Cu–30 at. %Al milled in: (a) planetary ball mill, (b) horizontal ball mill.

3.2.2. TEM observations

The 30 at. %Al powders presented more discrepancies between XRD and TEM. An outline of the phases observed is in Table 2. The analysis of the detection limits for each technique would be treated in the discussion section. As it could be noticed, 12 and 15 h of milling times were added in the TEM and XRD phase analysis of HM. The main reason of the addition of those times of milling would be developed in the description of Fig. 8 in the discussion section.

3.2.2.1. Planetary ball mill. For the sample 30-PM-10, TEM results showed consolidated particles composed by Cu and Al in accordance with XRD results. This is clearly inferred from the repetitive SAD patterns of Fig. 5(a) and from EDS studies. After 20 and 30 h milling, the presence of α and γ_2 phases appeared to be consistent with the results obtained by XRD and TEM. Fig. 5(b) shows an example of SAD pattern of the sample 30-PM-30. It was indexed considering α and γ_2 phases. However, a discrepancy between XRD analysis and SAD patterns identification was found in sample 30-PM-50. The indexation of peaks in XRD was consistent with the presence of α and γ_2 phases. SAD patterns showed a different result as presented in Fig. 5(c). As an example, ring assigned to the indexation 3 1 0 of the β phase could not be associated to either α or γ_2 phases. The rest of the rings are assigned to these phases.

3.2.2.2. Horizontal ball mill. At the shortest integrated milling time, TEM and X-ray results did not present discrepancies. For the sample 30-HM-10, particles observed were indexed considering only Cu and Al. However, the identification of the existing phases by TEM for samples 30-HM-12 and 30-HM-15 was not consistent with the results found by XRD. In addition to the SAD patterns that could be indexed considering α and γ_2 phases, there are rings that were consistent with the presence of Al. Increasing milling time up to 30 h led to a large compositional inhomogeneity between particles. Apart from considering α and γ_2 phases as in the previous cases, the presence of Al seemed to be needed to explain identities assigned to all rings as shown in the first SAD pattern presented in Fig. 6(a). For 30-HM-50, SAD patterns appeared to be consistent only with the presence of γ_2 phase. The same result was achieved with XRD. Finally, for the last step of milling, 30-HM-100, some of the obtained SAD patterns were indexed considering γ_2 and α_2 phases as shown in Fig. 6(b). However, it should be also pointed out that most of the particles showed a SAD pattern that could be indexed only taking into account the presence of γ_2 phase.

In addition, High Resolution TEM (HRTEM) images were obtained taking advantage of the TEM small resolution value. Fig. 7(a) shows a particle full of staking faults. A zoom of the dot square area is shown in Fig. 7(b). This area exhibits the typical AB staking sequence that could be associated to the compact phase γ′, also known as 2H. X-ray diffractogram is indexed taking into account the presence of γ_2 phase in 30-HM-100 sample. TEM techniques revealed the possible presence of two more phases, α_2 and γ. Both phases seemed to have lower mass ratio respect to γ_2 phase.

4. Discussion

4.1. Phase evolution of Cu–16 at. %Al

For this sample, TEM results detect the presence of Cu and Al after 10 h milling as shown in Fig. 3. The indexation of elemental blends and intermetallics is consistent for both XRD and TEM techniques in most of the cases. However, sample 16-PM-20 presents XRD peaks that could be associated to both Cu and Al. Instead, only α phase seems to be necessary to index SAD patterns. The peaks related to α are essentially the same as the Cu ones, except that they appear at lower 2θ values. This is due to the fact that the α phase is isostructural to Cu but with a larger lattice parameter. In this sample, most of the crystalline domains that produce the SAD patterns are smaller than 30 nm and belong to particles smaller than 2 μm. Meanwhile, the mean particle size of distribution of this sample is (80 ± 40) μm [33]. Compound identities from X-ray diffractogram peaks can be properly identified only when crystallite sizes are larger than 20 nm. For smaller domains, the peaks are too wide to allow a proper association between the phase and the corresponding peaks [26]. Then, the results seems to be consistent with the formation of α phase in smaller domains. Also the widening of XRD lines as the milling time increase is consistent with a spread of crystal domains sizes and internal tensions that could favor the formation of other phases. In addition, larger domains related to Cu and Al particles are too large to be analyzed by TEM. The typical thickness of Cu–Al samples that could be observed by TEM is under 500 nm [27]. Any crystallographic domain larger than that shows a black shadow in the image mode and produces no appreciable diffraction pattern. From these assumptions, it is concluded that larger domains seem to consume more milling time and energy to form an statistical amount of α phase large enough to be detected by XRD. Further discussion between the determination of crystal domains using direct observation of dark field images rather than indirect Rietveld method determination is developed and analyzed in [33].

According to XRD results, the same amount of time is required to obtain the intermetallic for both mills. However, the planetary ball milling is considered as a process that impinges a larger amount of energy to the system than the horizontal ball milling. This result might imply that the efficiency of the HM is higher than the PM for this composition. The up-right disposition of the chamber in HM associated to the gravity–magnetic enhanced balls movement seems to produce impacts that result in an effective fracture and rewelding to produce the α phase. On the contrary, the planetary movement of the balls in the chamber of the mill could favor the sliding motion between the balls and the particles. This process no necessarily produces the same amount of energy needed to achieve the final product. In addition, as it was mentioned by Kubasky et al. [34], the comparison between the results is meaningful even when the ball-to-powder ratios used for different mill type are not the same. This variable is not useful to compare results from different milling devices. Therefore, the formation of the interme-

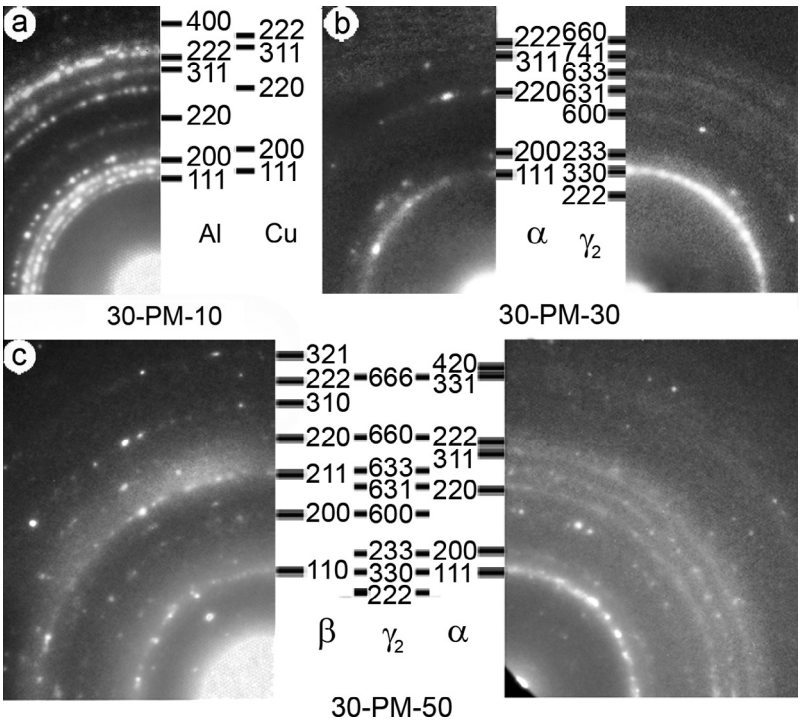

Fig. 5. Single quadrant TEM selected area diffraction of the samples obtained by PM (a) 30-PM-10, (b) 30-PM-30, (c) 30-PM-50.

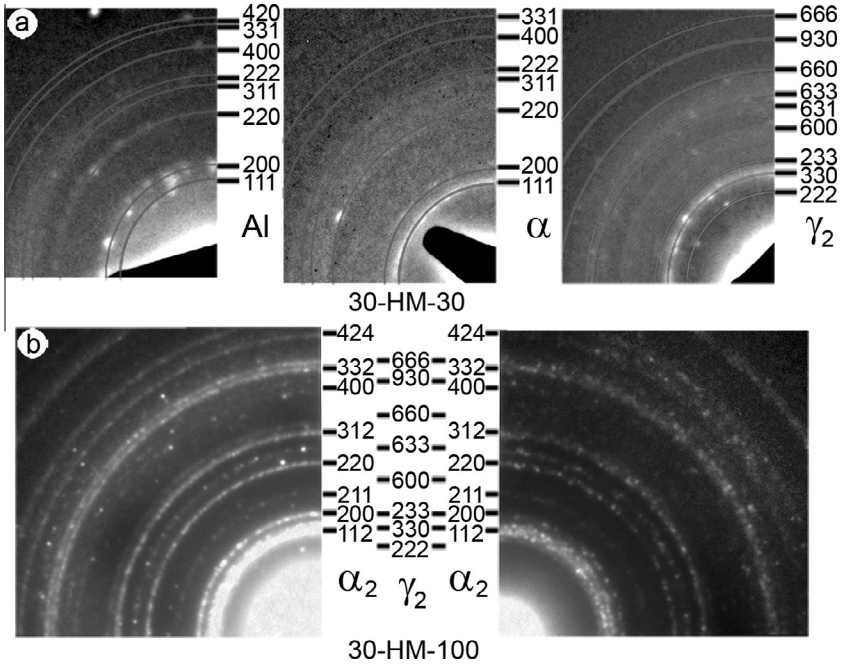

Fig. 6. Single quadrant TEM selected area diffraction of samples obtained by HM (a) 30-HM-30 (b) 30-HM-100.

tallic compound Cu–16 at. %Al seems to be more efficient in the HM than in the PM.

4.2. Phase evolution of Cu–30 at. %Al

Cu–30 at. %Al exhibits more discrepancies between the detectability of TEM and XRD techniques than samples with nominal composition Cu–16 at. %Al. Moreover, the phase evolution also exhibits more complicated development as the milling time increases. For this reason, the analysis of the results is separated into two subsections.

4.2.1. Phase detectability

Samples milled during 12, 15 and 30 h in the HM show SAD patterns that could be indexed considering the presence of an extra phase, Al, unobserved by XRD. It should be taken into account that the dark field images that confirm the size of the domains that produce SAD patterns are around 30 nm [33]. As it was mentioned in the Section 4.1, crystallographic domains of 30 nm could not

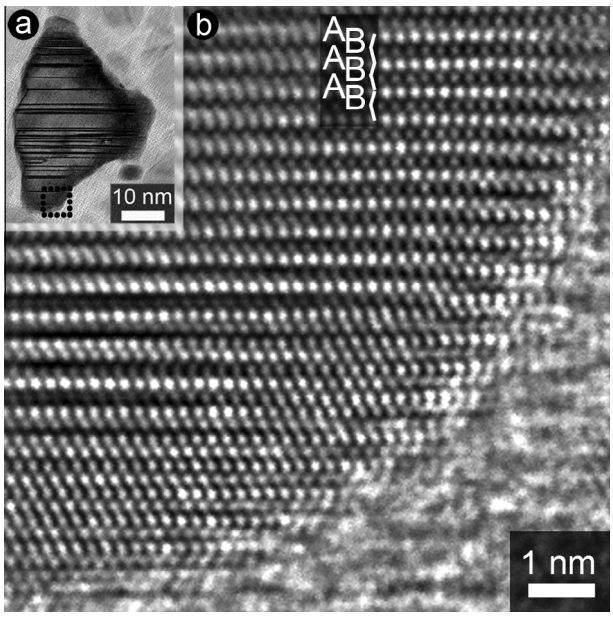

Fig. 7. (a) Bright field image of 30-HM-100. (b) HRTEM image of the square area in (a) showing γ′ phase.

produce sharps and defined peaks in a diffractogram. This effect could also be reinforced by the lower amount of Al in relation with the larger amount of mass of Cu.

Samples 30-PM-30, 30-PM-50, 30-HM-30, 30-HM-50 and 30-HM-100, present a SAD pattern that could be clearly indexed considering the presence of γ_2 phase. The rings that are attributed to other phases are either less bright or in some cases absent in some particles of the samples. Moreover, in sample 30-HM-50 all the SAD patterns are consistent only with the presence of one phase: γ_2. To study in detail this predominance, the phase evolution of γ_2 versus α is analyzed in Section 4.2.2.

Other detectability difference is observed in sample 30-PM-50. The possible existence of the metastable β phase could only be inferred using TEM. Since, any XRD peak could be associated unambiguously to this phase. In particular, due to TEM selectivity of the observed particles, it could be found a phase that appears with a low statistic presence not being massive enough to be detected by X-ray diffractograms. A similar situation occurs with the presumed detection of the γ′ phase only by HRTEM for 30-HM-100 sample. This phase could not be detected neither by XRD nor by SAD patterns. This may be associated to the low volume of this phase, not being able to produce SAD pattern. The presence of a low temperature phase in HRTEM image of a sample that presents a transformation temperature above room temperature was also reported in Ni–Al system [10]. Moreover, the presumed detection of γ′ phase in the last step of the most efficient milling type process would might reveal that a large amount of distortion achieved by ball hitting is required to form low temperature phase families. In addition to γ′ phase, SAD results seem to show the existence of α_2 phase while the XRD peaks appear to be associated only to γ_2 phase. The presence of γ_2 and α_2 phases, both predicted by the phase diagram, is not in agreement with the results showed on the diffractograms. From the XRD point of view, neither the planetary nor the horizontal mills give as a result the existence of α_2 phase. On the contrary, for PM, the α phase seems to be occurring, while this phase is not expected from the phase diagram. This last point could be related to the fact that the amount of energy needed to produce a replacement of Al in Cu structure producing α phase should be lower than the energy required to form γ_2 or α_2 phase. As it was mentioned in the introduction, γ_2 and α_2 phases have complex structures.

4.2.2. Kinetics of the main phase formation

Fig. 8 shows mass calculation from XRD patterns done by Rietveld method. The figure shows the evolution of the average mass percentage of α and γ_2 phases. Analysis for both mills is done by XRD because of the non statistical character of the TEM results. Nevertheless, it should not be forgotten XRD detectability limitation. Therefore, the phase evolution calculations were performed taking into account only the phases indicated by XRD in Table 2.

For the planetary mill and at 20 h, the largest mass percentage corresponds to α, reaching almost a 60% according to the Rietveld results. The same occurs at 30 h as shown in Fig. 8(a). However, after 50 h milling, the tendency changes and γ_2 phase narrowly exceeds the 50%. This point, corresponding to 30-PM-50, is identical to the one related to 30-HM-15 shown in Fig. 8(b). It means that milling for merely 15 h in the HM seems to be almost equivalent to milling 50 h in the PM. Moreover, since the increment of γ_2 phase in detriment of α phase occurred at shorter times for HM milling two extra samples were analyzed. The addition of the analysis of 12 and 15 h of milling develops the continuity in the evolution of the mass balance of α and γ_2 phases for HM. The equivalence in mass balance at 15 h in the HM and 50 h in the PM clearly reveals that the horizontal mill is the most efficient process for the system under study. To the point of obtaining a powder composed almost entirely by γ_2 phase after milling for 50 h in the HM. In the case of horizontal mill and according to Rietveld results, the increment of the average mass percentage of γ_2 phase occurs until the total disappearance of α. For planetary mill and even by milling for longer times, it is not possible to reach the same result. This effect could be attributed to a decay of mill efficiency after 50 h of milling.

The mass evolution according to Rietveld results shows that the α phase is formed first and γ_2 phase is formed second. This is reasonable considering the kinetics of the phase formation. At the beginning of milling, interactions seem to be Cu–Cu particles and Al–Cu particles due to 30 at. % of Al composition. Then, the Al–Cu interaction may favor the α phase formation before the γ_2 phase formation. In addition, the fact that Cu, Al and α phase are isostructural favors the early formation of α phase merely by the replacement of Cu atoms by Al atoms in the former structure. After that, milling progress allows the formation of one of the phases predicted by the equilibrium phase diagram: γ_2. A similar situation was observed for Ag–20 at. %Zn system where the ε phase with a HCP structure was detected in early integrated milling times of a high energy milling process. However, only the α phase, with an FCC structure, is stable in the Ag–Zn solid solution for this composition [35]. Eventhough only the α phase remains after the final milling process, the system found energetically convenient to form ε phase first. This phase is isostructural with Zn.

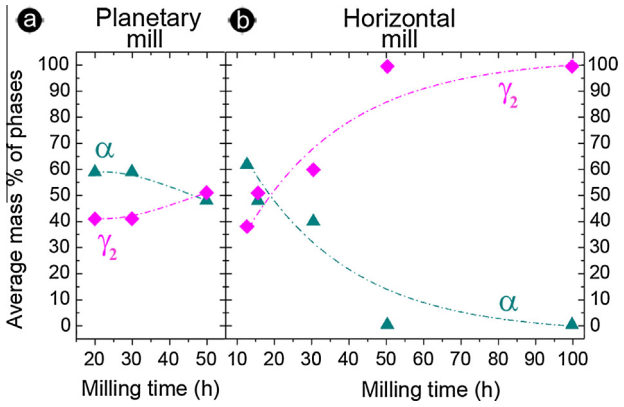

Fig. 8. Evolution of the average mass% of α and γ_2 phases during milling, for (a) planetary mill and (b) horizontal mill, with an error of ±2%.

Table 3
Lattice parameter obtained for α and γ_2 phases by Rietveld method.

Lattice parameter (± 0.001 Å)		
Sample	Phase	
	α	γ_2
30-PM-20	3.622	8.726
30-PM-30	3.617	8.726
30-PM-50	3.616	8.711
30-HM-15	3.618	8.714
30-HM-30	3.628	8.716
30-HM-50	–	8.731
30-HM-100	–	8.700

Most of the implications that appears in this paragraph are based in the idea that, the higher the content of aluminum in α phase, i.e. moving towards to the right in the phase diagram presented in Fig. 1, the larger the lattice parameter of the α phase. From Rietveld method, it was obtained the refined lattice parameters of the phases for each t_{im}. The most representative results are shown in Table 3. On the one hand and regarding planetary milling, where XRD patterns are consistent only with the presence of α and γ_2 phases, the increment in mass percentage of γ_2 seems to happen at the expense of obtaining Al atoms from the α phase. The decrement in the α lattice parameter is indicative of a possible reduction in the Al content of this phase. This reduction would enable the γ_2 mass percentage increment. On the other hand, the case of horizontal milling is not the same. For HM and according to Rietveld results, a growth of the lattice parameter of α phase is observed from 3.618 Å for 15 h to 3.628 Å for 30 h milling. The difference between the two mills could be attributed to the fact that for HM until 30 h milling it is still possible to find pure aluminum by TEM. This presence allows the possibility of increase both the Al content in α phase and the average mass percentage of γ_2 phase. Once Al and α phase seem to be disappeared, γ_2 lattice parameter still varies, from 8.731 Å for 30-HM-50 to 8.700 Å for 30-HM-100. This could be explained from TEM results where the presence of new phases, α2 and γ′, is consistent with the indexation of the SAD patterns. It denotes that the system could be still evolving and γ_2 lattice parameter seems to be not constant during these t_{im}.

Since the microstructure observed by TEM is not consistent with nucleation and growth, it is assumed that the phase formation is due to diffusion through the grain boundaries. Being the case, the diffusion between neighboring structures closer in symmetry group might explain the suppression of the α_2 formation. The structure of α belongs to the *Fm*3*m* space group and the structure of γ_2 belongs to the *P*-43*m* space group. Those structures are within the same symmetry subgroup (*Fm*3*m*) [36]. Instead, α_2 belongs to the *I*4/*mmm*. This is a subgroup within a different symmetry subgroup of lower order. Under the limited diffusion conditions, it seems reasonable that the system might favor the kinetics of formation of structures closer in symmetry instead of favoring the formation of structures having a larger difference in inherent symmetry.

5. Conclusions

A stable Cu–Al solid solution can be obtained for Cu–16 at. %Al and Cu–30 at. %Al by two different ball milling processes. Only α phase, the stable phase according the phase diagram, was obtained by reactive milling of Cu–16 at. %Al. On the contrary, the intermetallics detected in the last step of planetary milling of Cu–30 at. %Al were not in total agreement with the equilibrium phases present on the phase diagram.

The existence of low temperature γ′ and high temperature β was detected by TEM in the last steps of milling processes for Cu–30 at. %Al. In addition to the γ′ phase observed by HRTEM for the most efficient milling type process and a composition of 30 at. %Al, the equilibrium phases γ_2 and α_2 were detected by TEM.

The formation of α_2 might be hindered because the kinetic of the process is governed by diffusion through the grain boundaries and it might induce the creation of structures that belongs to the same symmetry subgroup. That is the case for α and γ_2. Instead, α_2 structure belongs to a different symmetry subgroup.

The achievement of the intermetallic compound of equilibrium for both compositions seems to be more efficient with the horizontally-motioned mill.

Acknowledgments

The authors express their thanks to Consejo Nacional de Investigaciones Científicas y Técnicas (CONICET), to Agencia Nacional de Promoción Científica y Tecnológica (ANPCyT: PICT-2011-0643 and PICT-2011-0092) and to Comisión Nacional de Energía Atómica (CNEA) for supporting this work. Dr. Marcos Sade is gratefully acknowledged for fruitful discussion.

References

[1] C. Suryanarayana, Non-Equilibrium Processing of Materials, Pergamon Press, Oxford, 1999.
[2] K. Upadhya, Plasma Synthesis and Processing of Materials, TMS, Warrendale, PA, 1993.
[3] H.H. Liebermann, Rapidly Solidified Alloys: Processes, Structures, Properties, Applications, Marcel Dekker, New York, NY, 1993.
[4] T.R. Anantharaman, C. Suryanarayana, Rapidly Solidified Metals – A Technological Overview, Trans Tech Publications, Aedermannsdorf, Switzerland, 1987.
[5] R.L. Bickerdike, D. Clark, J.N. Easterbrook, G. Hughes, W.N. Mair, P.G. Partridge, H.C. Ranson, Microstructure and tensile properties of vapor deposited aluminum alloys, Part I: Layered microstructures, Int. J. Rapid Solidification 1 (1984–1985) 305–325.
[6] C. Suryanarayana, Mechanical alloying and milling, Prog. Mater Sci. 46 (2001) 1–184.
[7] M.A. Dvorack, N. Kuwano, S. Polat, Haydn Chen, C.M. Wayman, Decomposition of a β_1-phase Cu–Al–Ni alloy at elevated temperature, Scr. Metall. 17 (11) (1983) 1333–1336.
[8] S.K. Pabi, B.S. Murty, Mechanism of mechanical alloying in Ni–Al and Cu–Zn systems, Mater. Sci. Eng., A 214 (1996) 146–152.
[9] V.K. Portnoy, A.M. Blinov, I.A. Tomilin, V.N. Kuznetsov, T. Kulik, Formation of nickel aluminides by mechanical alloying and thermodynamics of interaction, J. Alloys Compd. 336 (2002) 196–201.
[10] E. Zelaya, M.R. Esquivel, D. Schryvers, Evolution of the phase stability of Ni–Al under low energy ball milling, Adv. Powder Technol. 24 (2013) 1063–1069.
[11] M. Jafari, M.H. Abbasi, M.H. Enayati, F. Karimzadeh, Mechanical properties of nanostructured Al2024–MWCNT composite prepared by optimized mechanical milling and hot pressing methods, Adv. Powder Technol. 23 (2012) 205–210.
[12] A. Evirgen, M.L. Övecoglu, Characterization investigations of a mechanically alloyed and sintered Al–2 wt%Cu alloy reinforced with WC particles, J. Alloys Compd. 496 (2010) 212–217.
[13] T. Shanmugasundaram, M. Heilmaier, B.S. Murty, V. Subramanya Sarma, On the Hall–Petch relationship in a nanostructured Al–Cu alloy, Mater. Sci. Eng., A 527 (2010) 7821–7825.
[14] N. Nemati, R. Khosroshahi, M. Emamy, A. Zolriasatein, Investigation of microstructure, hardness and wear properties of Al–4.5 wt.% Cu–TiC nanocomposites produced by mechanical milling, Mater. Des. 32 (2011) 3718–3729.
[15] S. Samal, B. Satpati, D. Chaira, Production and dispersion stability of ultrafine Al–Cu alloy powder in base fluid, J. Alloys Compd. 504S (2010) 389–394.
[16] T.B. Massalski, J.L. Murray, L.H. Bennett, H. Baker, Binary Alloy Phase Diagrams, vol. 1 and 2, American Society for Metals, Metals Park, OH, 1986.
[17] P.R. Swann, H. Warlimont, The electron-metallography and crystallography of copper–aluminum martensites, Acta Metall. 11 (6) (1963) 511–527.
[18] G. Roulin, P. Duval, Initial stages of ordering obtained by tempering of disorder martensitic phase of Cu–Al alloys, Scr. Mater. 37 (1997) 45–51.
[19] S. Westman, Refinement of the gamma-Cu9Al4 structure, Acta Chem. Scand. 19 (1965) 1411–1419.
[20] T.B. Massalski, The Al–Cu (aluminum–copper) system, J. Phase Equilib. 1 (1) (1980) 27–33.
[21] H. Sato, R.S. Toth, G. Honjo, Remarks on the structure of martensites in Cu–Al alloys, Acta Metall. 15 (8) (1967) 1381–1396.
[22] F.C. Lovey, The fault density in 9R type martensites: a comparison between experimental and calculated results, Acta Metall. 35 (5) (1987) 1103–1108.
[23] Z. Nishiyama, J. Kakinoki, S. Kajiwara, Stacking fault in the martensite of Cu–Al alloy, J. Phys. Soc. Jpn. 20 (7) (1965) 1192–1211.

[24] S.M. Tang, C.Y. Chung, W.G. Liu, Preparation of Cu–AI–Ni-based shape memory alloys by mechanical alloying and powder metallurgy method, J. Mater. Process. Technol. 63 (1997) 307–312.
[25] S.K. Vajpai, R.K. Dube, S. Sangal, Application of rapid solidification powder metallurgy processing to prepare Cu–Al–Ni high temperature shape memory alloy strips with high strength and high ductility, Mater. Sci. Eng., A 570 (2013) 32–42.
[26] A. Guinier, D.L. Dexter, X-Ray Studies of Materials, Interscience Publishers, 1963.
[27] D.B. Williams, C.B. Carter, Transmission Electron Microscopy – A Textbook for Materials Science, Springer, 2009.
[28] J. Kano, M. Miyazaki, F. Saito, Ball mill simulation and powder characteristics of ground talc in various types of mill, Adv. Powder Technol. 11 (3) (2000) 333–342.
[29] J. Lee, Grinding effects on the change of particle properties in cupric sulfide, CuS, Adv. Powder Technol. 23 (6) (2012) 731–735.
[30] S.A. Obregón, J.J. Andrade Gamboa, M.R. Esquivel, Synthesis of Al-containing MmNi5 by mechanical alloying: milling stages, structure parameters and thermal annealing, Int. J. Hydrogen Energy 37 (19) (2012) 14972–14977.
[31] J. Rodriguez-Carvajal, Satellite meeting on powder diffraction, in: Proc. of the Fifteenth Conference of the International Union of Crystallography, Toulouse, France, vol. 127, 1990.
[32] J. Rodriguez-Carvajal, Recent developments of the program FULLPROF, Comm. Powder Diffr. (IUCr) 26 (2001) 12–19.
[33] M.F. Giordana, N. Muñoz Vásquez, M.R. Esquivel, E. Zelaya, Unpublished results.
[34] E.T. Kubaski, O.M. Cintho, J.L. Antoniassi, H. Kahn, J.D.T. Capocchi, Obtaining NiAl intermetallic compound using different milling devices, Adv. Powder Technol. 23 (2012) 667–672.
[35] D. Guzmán, O. Rivera, C. Aguilar, S. Ordoñez, C. Martínez, D. Serafini, P. Rojas, Mechanical alloying and subsequent heat treatment of Ag–Zn powders, Trans. Nonferrous Met. Soc. China 23 (2013) 2071–2078.
[36] C. Giacovazzo, Fundamentals of Crystallography, Oxford University Press, 2002.